3D numerical simulation of debris-flow motion using SPH method incorporating non-Newtonian fluid behavior

Wei Wang[1,2] · **Guangqi Chen**[1] · **Zheng Han**[1,3] ·
Suhua Zhou[1] · **Hong Zhang**[1] · **Peideng Jing**[1]

Abstract Flow-type landslide, such as debris-flow, often exhibits high velocity and long run-out distance. Simulation on it benefits the propagation analysis and provides solution for risk assessment and mitigation design. Previous studies commonly used shallow water assumption to simulate this phenomenon, ignoring the information in vertical direction, and the Bingham model to describe constitutive law of non-Newtonian fluid can cause numerical divergence unless necessary parameter is defined. To address the issue, the full Navier–Stokes equations are adopted to describe the dynamics of the flow-type landslides. Additionally, the general Cross model is employed as the constitutive model, which ensures the numerical convergence. Rheological parameters are introduced from the Bingham model and the Mohr–Coulomb yield criterion. Subsequently, the governing equations incorporating the modified rheological model are numerically built in the smoothed particle hydrodynamics (SPH) framework and implemented into the open-source DualSPHysics code. To illustrate its performance, the 2010 Yohutagawa debris-flow event in Japan is selected as a case study. Parameters regarding the debris magnitude, i.e., the front velocity and section discharge, were also well analyzed. Simulated mass volume and deposition depth at the alluvial fan are in good agreements with the in situ observation. On the basis of the results, the developed method performs well to reproduce the debris-flow process and also benefits the analysis of flow characteristics, affected area for risk assessment and mitigation design.

✉ Zheng Han
  hankzzz@163.com

1 Department of Civil and Structural Engineering, Kyushu University, Fukuoka 819-0395, Japan

2 Faculty of Engineering, China University of Geosciences (Wuhan), Wuhan 430074, China

3 School of Civil Engineering, Central South University, Changsha 410075, China

1 Introduction

Debris-flow is gravity-driven, mixed with water and highly concentrated with sediment commonly composited by poorly sorted rock, soil, organic matter and sundry debris (Major 1997). The phenomena exhibit extremely large deformation that transfers of even boulder-rich debris through tortuous channels, across gentle slopes and around obstructions (Iverson 1997). Many researchers define debris-flow as a flow-type landslide (Hungr et al. 2001; McDougall and Hungr 2004; Cola et al. 2008; Huang et al. 2012; Pastor et al. 2014) as they share similar features (e.g., large volume of loosen materials, high velocity of motion and long run-out distance). The occurrence of debris-flow usually accompanies with a great number of casualties and widespread damages (Cascini et al. 2012; Han et al. 2014a). Catastrophic debris-flow events occur pervasively, such as 1997 Dolomites event (Berti et al. 1999) and Sarno event in 1998 (Crosta and Dal Negro 2003) in Italy, the Hiroshima event of Japan in 1999 (Wang et al. 2003), the 2002 Rossiga event in Italy (Sosio et al. 2007) and the 2010 Zhouqu debris event in China (Tang et al. 2011).

For debris-flow research, most of studies focus on the flow motion analysis in terms of run-out distance and flow velocity. The motivation for those kinds of analysis is to define the hazardous region where can be possibly impacted by the flow and to evaluate the intensity of the disaster for hazard and risk assessment. The dynamic analysis of the debris-flow also benefits the mitigation design as well as the hazard prevention strategies (Fell et al. 2008). However, the debris-flow motion is difficult to analyze because the distinctive features of mechanical vary from case to case, and relevant rheological parameters cannot be simply measured in full-scale examples (Huang et al. 2012; Cascini et al. 2014). The analytical difficulties even remain due to the rough complicated terrains and long distance of the debris-flow catchment.

Aiming to analyze the flow propagation, several methods have been developed in recent years. They can be categorized into three major kinds, i.e., empirical method, physical modeling and analytical solution. Respect for empirical method, data from the field investigations are the key input to propose empirical equations for the prediction purpose. For instance, the relationship among debris volume, run-out distance and local morphology can be empirically summarized if sufficient historical data are available. Since now, these empirical methods provide straightforward ways to estimate debris run-out distance correlated with the amount of unstable volume (Corominas 1996); to determine the peak discharge, the mean flow velocity, the total travel distance following the assessment of debris-flow volume (Rickenmann 1999; Han et al. 2014a); to predict the entrainment and deposition together with multiple variables including incoming flow volume, slope angle and bend-angle function (Fannin and Wise 2001); to define the mobility coefficient as a function of geomorphologic catchment parameters (Scheidl and Rickenmann 2010). It is worth noting that the empirical method is able to capture the global observed behavior (high mobility) of the debris-flow, while ignoring crucial local topography effects such as diversions or bifurcations (Cascini et al. 2014). Respect for the physical scale modeling, it has been widely used but limited by geometrical scale effects and financial issues (Chen and Lee 2000).

As regarded to the analytical solution, a couple of physically based equations are used to simulate the debris-flow movement based on either Eulerian-formulated model or Lagrangian framework. In Eulerian coordinates, velocity and debris depth can be alternatively obtained at each point of a given domain (Takahashi et al. 1992). However, from practical considerations, the Lagrangian framework is more suitable for these kinds of

problems because the computational grid may be distorted with the highly unsteady moving mass (Chen and Lee 2000). Therefore, the physically based mass and momentum equations are usually formulated in the Lagrangian frame to simulate flow-type landslides. In many cases, the governing equations are simplified by integrating the depth in the vertical direction, which makes the equation reduce from 3D to 2D. The so-called depth-integrated model has been widely used and widely adopted by engineering and earth scientists. The depth-integrated equations can be numerically solved by different schemes such as finite difference method (FDM) (O'brien et al. 1993; Wu et al. 2013; Han et al. 2013, 2015), finite element method (FEM) (Chen and Lee 2000), finite volume method (FVM) (Medina et al. 2008), smoothed particle hydrodynamics (SPH) (McDougall and Hungr 2004; Cola et al. 2008; Pastor et al. 2009, 2014; Cascini et al. 2013, 2014; Cuomo et al. 2014).

Nevertheless, the pressure and forces on structures may be not fully correct in depth-integrated model due to the limited information in vertical direction (Pastor et al. 2014). For more reliable results, the full Navier–Stokes (N–S) equations are suggested to describe the flow dynamic. Recently, the SPH method has been well applied to solve integral equations or partial difference equations (PDEs) in the field of computational fluid dynamics (CFD). This method is proved to be robust and reliable in modeling fluid dynamic with large deformation owing to the absence of computational grids or meshes as a Lagrangian particle-based method. A few elementary SPH applications for flow-type landslide solving the N–S equations have been proposed. As illustrated, Huang et al. (2011, 2012), Huang and Dai (2014) and Dai et al. (2014) used SPH method combined the Bingham constitutive model, to analyze the run-out of flow-type landslides as a kind of equivalent non-Newtonian fluid. Their studies indicate that the SPH modeling is able to obtain the fundamental dynamic behavior of the whole process. However, the effective viscosity in Bingham model may be infinite when shear rate approaching infinitesimally, which may result in numerical divergence. In addition, reproduction of the debris event across complex 3D terrain in high resolution is difficult to target, because huge amount of particles require much more computational time.

In this paper, the full N–S equations were used as the governing equations to describe the flow dynamic. Most importantly, we incorporated the non-Newtonian fluid model into the N–S equations to present the debris motion over 3D topography. In detail, the general Cross model (Barnes et al. 1989) was employed to present the rheological features of non-Newtonian fluid and ensure the numerical convergence. The rheological parameters were introduced from the more common Bingham model and the Mohr–Coulomb criterion. Then, the improved N–S equations were numerically solved by the SPH method in three-dimensional scheme, and coded in DualSPHysics (available on http://dual.sphysics.org/) which is a SPH-based open-source package (Crespo et al. 2011, 2015). As a case study, the potentialities and drawbacks of the application were verified by reproducing the Yohuta-gawa debris-flow event occurred in October 20, 2012, in Amami Oshima, Japan.

2 SPH method

Smoothed particle hydrodynamics is a "truly" mesh-free, particle-based method originally used for continuum scale applications (Liu and Liu 2010). It has been decades since the SPH method was firstly proposed in 1977 to solve the astrophysical problems in three-dimensional open space (Lucy 1977; Gingold and Monaghan 1977), since the collective

movement of those particles is similar to the movement of a liquid or gas flow, and it thus can be applied to deal with the fluid dynamics (Monaghan 1988; Liu and Liu 2010). In SPH method, the fluid and continuum media are treated as a set of discretized particles. The integration of the equations to describe the motion of fluid is solved in the Lagrangian formalization. Any physical variables (e.g., density, pressure, velocity, position) of a particle can be approximated by the values of the surrounding particles with a kernel function. It is the kernel approximation and particle discretization that make SPH method to be greatly capable to tackle the problem with free surface flow and large deformation but without grids [details can be found in Monaghan (1992) and Liu and Liu (2010)]. Recent improvements in SPH method are also remarkable, such as the incompressible SPH (ISPH) (Morris et al. 1997; Lee et al. 2008; Shao 2010; Liu et al. 2014); laminar viscosity and sub-particle scale turbulence (LSPS) terms (Gotoh et al. 2004; Dalrymple and Rogers 2006) and a new density diffusion term named delta-SPH (Molteni and Colagrossi 2009). Here we only present the main features and numerical techniques used in this simulation.

Supposing a function $f(x)$ at any point x, the fundamental principle is to approximate it in the way:

$$f(x) \cong \int_{\Omega} f(x')W(x - x', h)dx' \tag{1}$$

where h is the smoothing length which indicates the interaction distance of particles over the weighting function $W(x - x', h)$. Ω is the support domain determined by smoothing length h. The integration in point i then is derived by the summation of a set of particles included in the support domain, which is named particle discretization. The discrete form of Eq. (1) is described as:

$$f(x_i) = \sum_{j=1}^{N} m_j \frac{f(x_j)}{\rho_j} W_{ij} \tag{2}$$

where m_j and ρ_j are the mass and density of particle j, respectively, and $W_{ij} = W(x_i - x_j, h)$ indicates the smoothing function of particle i evaluated at particle j. With the same manner, the derivation of a function can be expressed in the discrete form like:

$$\frac{df(x)}{dx_i} = -\sum_{j=1}^{N} m_j \frac{f(x_j)}{\rho_j} \frac{\partial W_{ij}}{\partial x_i} \tag{3}$$

There are a couple of kernel functions available. Usually, the accuracy of the computation increases with the high-order kernel function while significant time is necessary. Here, we choose the quantic Wendland kernel:

$$W(x - x', h) = \alpha_D \left(1 - \frac{q}{2}\right)^4 (2q + 1); \quad 0 \le q \le 2 \tag{4}$$

where $q = |x - x'|/h$ and α_D is $7/(4\pi h^2)$ in 2D and $21/(16\pi h^3)$ in 3D. The movement of fluid is described as the N–S equations which consist of the continuity and momentum equations:

$$\frac{d\rho}{dt} = -\rho \frac{\partial v^\beta}{\partial x^\beta} \tag{5}$$

$$\frac{\mathrm{d}v^\alpha}{\mathrm{d}t} = \frac{1}{\rho}\frac{\partial \sigma^{\alpha\beta}}{\partial x^\beta} + g^\alpha \tag{6}$$

where ρ is the density; α and β are used to denote the coordinate directions in three-dimensional space; v^β presents the particle velocity; $\sigma^{\alpha\beta}$ denotes the total stress tensor and g^α (0, 0, -9.81 m/s^2) is the gravity acceleration. In SPH notation, Eqs. (5) and (6) can be rewritten as:

$$\frac{\mathrm{d}\rho_i}{\mathrm{d}t} = \sum_{j=1}^{N} m_j \left(v_i^\beta - v_j^\beta \right) \frac{\partial W_{ij}}{\partial x_i^\beta} \tag{7}$$

$$\frac{\mathrm{d}v_i^\alpha}{\mathrm{d}t} = \sum_{j=1}^{N} m_j \left(\frac{\sigma_i^{\alpha\beta}}{\rho_i^2} + \frac{\sigma_j^{\alpha\beta}}{\rho_j^2} \right) \frac{\partial W_{ij}}{\partial x_i^\beta} + g^\alpha \tag{8}$$

As known in the SPH formulations for weakly compressible fluid, the pressure field generally presents instability and numerical noise due to the approximation of the density. Especially, the noise of the pressure field could be particularly critical in the present case due to the use of a Mohr–Coulomb criterion through which the effective viscosity of the material and the pressure are explicitly coupled. To deal with this problem, the delta-SPH method was adopted. The delta-SPH method (Molteni and Colagrossi 2009), or named the artificial density diffusion, implemented by adding a diffusive term in the continuity Eq. (7), has the type of:

$$D_i = \xi h c_0 \sum_{j=1}^{N} \psi_{ij} m_j \cdot \frac{\partial W_{ij}}{\partial x_i^\beta} \tag{9}$$

where ξ is a free parameter adopted 0.1; c_0 is the speed of sound at reference density; ψ_{ij} is written:

$$\psi_{ij} = 2(\frac{\rho_i}{\rho_j} - 1)\frac{\left(x_i^\beta - x_j^\beta \right)}{\left| x_i^\beta - x_j^\beta \right|^2 \varepsilon_h h^2} \tag{10}$$

where ε_h is a small constant adopted 0.01 usually. By introducing the density diffusion term, the continuity Eq. (7) has the form as:

$$\frac{\mathrm{d}\rho_i}{\mathrm{d}t} = \sum_{j=1}^{N} m_j \left(v_i^\beta - v_j^\beta \right) \frac{\partial W_{ij}}{\partial x_i^\beta} + \xi h c_0 \sum_{j=1}^{N} \psi_{ij} m_j \cdot \frac{\partial W_{ij}}{\partial x_i^\beta} \tag{11}$$

As regarded to the momentum Eq. (8), the total stress tenor can be written as the summation of an isotropic component pressure p and a viscous shear stress component $\tau^{\alpha\beta}$.

$$\sigma^{\alpha\beta} = -p\delta^{\alpha\beta} + \tau^{\alpha\beta} \tag{12}$$

where $\delta^{\alpha\beta}$ is the Kronecker delta function. Substituting Eq. (12) into the momentum Eq. (8), yielding:

$$\frac{\mathrm{d}v_i^\alpha}{\mathrm{d}t} = -\sum_{j=1}^{N} m_j \left(\frac{p_i}{\rho_i^2} + \frac{p_j}{\rho_j^2} \right) \frac{\partial W_{ij}}{\partial x_i^\alpha} + \sum_{j=1}^{N} m_j \left(\frac{\tau_i^{\alpha\beta}}{\rho_i^2} + \frac{\tau_j^{\alpha\beta}}{\rho_j^2} \right) \frac{\partial W_{ij}}{\partial x_i^\beta} + g^\alpha \tag{13}$$

Here, the first term of the right-hand side represents the SPH approximation for the pressure term, while the second one implies the acceleration due to the viscous force. The pressure term is computed using an appropriate Equation of State (EoS) which relates the hydrostatic pressure to local densities.

$$p = B\left[\left(\frac{\rho}{\rho_0}\right)^{\gamma} - 1\right] \tag{14}$$

where constant $B = c_0^2\rho_0/\gamma$, ρ_0 is the reference density, c_0 is the speed of sound at reference density calculated by $\beta(gh_{\max})^{1/2}$, β is a constant accepted 10 here and γ is a dimensionless parameter usually taken as 7.

3 Rheological model

In the original DualSPHysics code (version 3.0), it is robust in dealing with the Newtonian fluid such as the water flow, but impossible to cope with the non-Newtonian flow. To make it possible for the debris-flow simulation, relevant rheological model should be implemented in the original code. This section introduces the implementation of the constitutive law in detail.For Newtonian incompressible fluid, the shear stress tensor can be calculated in the form:

$$\tau^{\alpha\beta} = \mu\varepsilon^{\alpha\beta} \tag{15}$$

where $\varepsilon^{\alpha\beta}$ is the local strain rate tensor, μ is the dynamic viscosity treated as a constant value for Newtonian fluid, while the features of flow-like landslides are way different. According to Ancey (2007), rapid mass movements such as the avalanches or debris-flow involving slurries of solid particles within an interstitial fluid can be modeled as plastic materials defined by either Coulomb plasticity or viscoplasticity. In addition, the post-yielding behavior is usually properly characterized depending on the material properties and flow features. As for the debris-flow, it involves complicated problems with extremely large deformation, in which the strain rate is far more than 100 % (Dai et al. 2014). Besides, Hadush et al. (2000) summarized the relationship between viscosity and shear rate based on three different measurement methods. The results showed this relationship in high deformed soil material is in good agreements with the non-Newtonian fluid dominated by viscoplasticity. In non-Newtonian fluid, the viscosity is dependent on the shear rate or shear rate history. The relationship between the shear stress tensor $\tau^{\alpha\beta}$ and shear rate tensor $\varepsilon^{\alpha\beta}$ of non-Newtonian fluid can be expressed as:

$$\tau^{\alpha\beta} = \tau^{\beta\alpha} = \mu_{\mathrm{eff}}\varepsilon^{\alpha\beta} \tag{16}$$

where μ_{eff} is the effective viscosity varying with time and $\varepsilon^{\alpha\beta}$ is defined as:

$$\varepsilon^{\alpha\beta} = \frac{1}{2}\left(\frac{\partial v^{\alpha}}{\partial x^{\beta}} + \frac{\partial v^{\beta}}{\partial x^{\alpha}}\right) \tag{17}$$

Substituting Eq. (16) into the former momentum Eq. (13), we have the new equation incorporating the total stress of non-Newtonian fluid:

$$\frac{\mathrm{d}v_i^{\alpha}}{\mathrm{d}t} = -\sum_{j=1}^{N} m_j\left(\frac{p_i}{\rho_i^2} + \frac{p_j}{\rho_j^2}\right)\frac{\partial W_{ij}}{\partial x_i^{\alpha}} + \sum_{j=1}^{N} m_j\left(\frac{\mu_{\mathrm{eff}i}\varepsilon_i^{\alpha\beta}}{\rho_i^2} + \frac{\mu_{\mathrm{eff}j}\varepsilon_j^{\alpha\beta}}{\rho_j^2}\right)\frac{\partial W_{ij}}{\partial x_i^{\beta}} + g^{\alpha} \tag{18}$$

The key point to describe the dynamics of non-Newtonian fluid using Eq. (18) is to evaluate the effective viscosity varying with shear rate. The simplest constitutive law to describe the non-Newtonian behavior of extremely large deformation of soil materials would be the Bingham model (Komatina and Jovanovic 1997; Hadush et al. 2000; Naili et al. 2005; Hosseini et al. 2007). As for the Bingham model, the fluid is capable of resisting any shear stress under the yield stress and preforms as "solid" does. When excessing the yield stress, the material behaves as the Newtonian flow driven by the excess of the shear stress beyond the yield stress. Once again the shear stress falls below the yield stress, the materials' movements are frozen and there is either plug flow or no flow at all. The effective viscosity of Bingham model can be written as:

$$\mu_{\text{eff}} = \mu_{\text{B}} + \frac{\tau_{\text{B}}}{\dot{\gamma}} \tag{19}$$

where μ_{B} is the Bingham viscosity and τ_{B} is yield stress; $\dot{\gamma}$ is defined as the second invariant of the shear rate tensor $\varepsilon^{\alpha\beta}$:

$$\dot{\gamma} = \sqrt{\frac{1}{2}\varepsilon^{\varepsilon\beta} \cdot \varepsilon^{\varepsilon\beta}} \tag{20}$$

Provided in the condition of shear rate, $\dot{\gamma} \to 0$, μ_{eff} in Bingham model will approach an infinite value, and thus, straightforward computation is not possible. For this reason, previous studies used varies kind of regularized Bingham model to avoid the numerical divergence, i.e., the simple regularization (Frigaard and Nouar 2005), the threshold regularization (Laigle et al. 2007). While in this study, the general Cross model (Barnes et al. 1989) was selected to present the non-Newtonian behavior of the flow-type landslide

$$\mu_{\text{eff}} = \frac{\mu_0 + (K\dot{\gamma})^m \mu_\infty}{1 + (K\dot{\gamma})^m} \tag{21}$$

where μ_0 and μ_∞ are the viscosity of fluid at very low and high shear rates, respectively; K and m are constant parameters. Obviously, the effective viscosity is determined by four parameters which are not easy to obtain in the Cross model. For convenience, we adopted the approach proposed by Shao and Lo (2003) who worked out these parameters by introducing the more common Bingham fluid parameters. Taking $m = 1$ in Eq. (21), we get the effective viscosity in the Cross model as:

$$\mu_{\text{eff}} = \frac{\mu_0 + K\mu_\infty\dot{\gamma}}{1 + K\dot{\gamma}} \tag{22}$$

In most situation, $K\dot{\gamma} >> 1$, comparing the Eq. (19) with Eq. (22), the other two unclear parameters in the Cross model can be obtained as:

$$\mu_\infty = \mu_{\text{B}} \tag{23}$$

$$K = \frac{\mu_0}{\tau_{\text{B}}} \tag{24}$$

Respect for the material in geotechnical engineering, the yield stress of which is commonly defined as the Mohr–Coulomb yield criterion with the cohesion c and frictional angle φ (Huang et al. 2011, 2012; Dai et al. 2014) as:

$$\tau_B = c + \sigma \tan \varphi \tag{25}$$

where σ is the pressure. By applying the above manner, the only unknown factor in the Cross model is the viscosity coefficient under low shear rate μ_0. Particularly, Hammad and Vradis (1994) suggested that the accuracy of the numerical solution is not very related to the above high value once the viscosity at low shear rate is 1000 times larger than that at high shear rate.

$$\mu_0 = 1000\mu_\infty \tag{26}$$

By introducing the Bingham parameters into the Cross model, the effective viscosity is able to continuous vary with $\dot{\gamma}$ even it equals to zero. Figure 1 shows the effective viscosity against shear rate for the Cross model, exact Bingham model and regularized Bingham models (Frigaard and Nouar 2005; Laigle et al. 2007). Note that in the low shear range, the effective viscosity of the exact Bingham model tends to the infinite value as compared to other three models. In the rest three models, the result of Cross model is the closest one to the exact Bingham model but without numerical divergence.

4 Case study

The Yohutagawa torrent (28°24′N, 129°32′E) located in the Amami Oshima Island, southwest Japan has a catchment area of about 0.24 km^2 and elevation varying from 20 to 250 m. Figure 2a shows the location of the Yohutagawa torrent. From the geological viewpoint, the strata in this region are mainly composited by sandstone and mudstone showed in Fig. 2b. While the colluvium deposits lying above the bedrock has a typically few meters thick, consisting by clayey matrix mixed with the highly fragmented plates of sandstone and mudstone. Before the occurrence of the Yohutagawa debris event, large
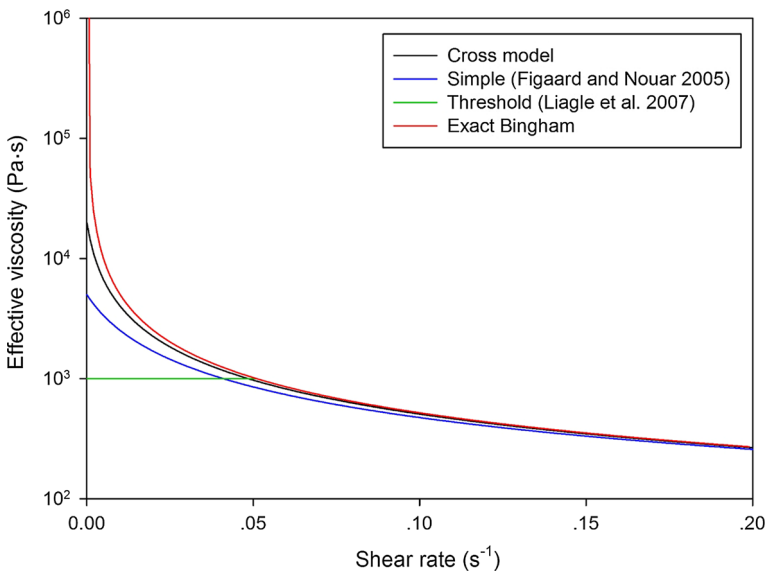
Fig. 1 Effective viscosity against shear rate of different rheological model for parameters ($\mu_B = 20$ Pa·s, $\tau_B = 50$ Pa)
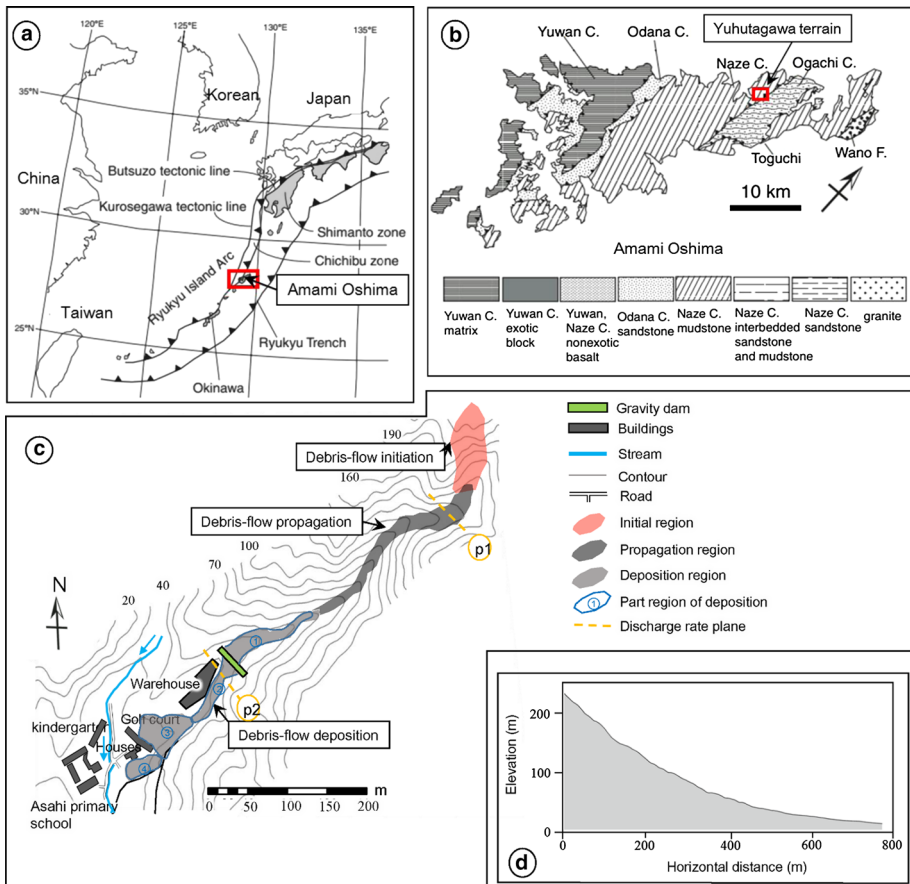
Fig. 2 Main features of the 2010 Yohutagawa debris-flow event. **a** Location of the Amami Oshima, **b** geological settings of the Amami Oshima area and location of the Yohutagawa gully, modified from Osozawa et al. (2009), **c** layout of the Yohutagawa debris-flow and corresponding infrastructures, modified from Han et al. (2015), **d** typical cross section of the Yohutagawa gully

portion of the catchment was covered by the vegetation. Moreover, the catchment has an average slope angle of about 16° ranging from 33° in the upper part to 5° of the alluvial fan (Wu et al. 2013; Han et al. 2014b). The total length of the channel is approximately 800 m as shown in Fig. 2d.

The 2010 Yohutagawa debris-flow event was triggered by an intensive rainfall accompanying with Typhoon Meji in October 2010. Especially, the rainfall in this event is termed to be the most intensive one sustaining from 18 to 20 October with an accumulated intensity of 601 mm, while the maximum intensity per hour is recorded as 73 mm between 15:00 and 16:00 in 20 October. Soon after the 73 mm rainfall in an hour, the colluvium deposit in the source area initiated. The source was composited of highly fragmented sandstone and mudstone mixing with clay matrix. The debris-flow travelled about 1100 m along the channel and deposited at the alluvial fan downstream. Majority of the debris mass was intercepted by a check dam near the outlet of the channel, and only few mass overpassed the dam, damaging two buildings at the alluvial fan (Fig. 2c).

A field investigation was conducted by the Kokusai Kogyo Group (KKG) right after the event. The main features of the debris-flow are shown in Fig. 2c as well as the relevant photographs in Fig. 3. The geological survey reveals that the debris-flow was initiated in the upper part of the Yohutagawa gully, propagated about 800 m along the channel and finally deposited before and beyond the gravity dam. Field investigation indicates that the debris source is approximately 8697 m^3 with average depth of 3.75 m, the volume inter-cepted by the dam is about 5,621 m^3, and the deposition volume is estimated to be 3076 m^3. Figure 3 shows that the kinder garden and the primary school near the site are not affected because of the existence of the dam constructed in 1982.

The proposed method in the paper is used to simulate the Yohutagawa debris-flow over the 3D topography, and the propagation and deposition features of this event can be studied. In this case, the 3D topography is composed by a vast number of triangles derived from the original DEM data with the scale of 1/2000. Then, the previous generated triangles are transformed into a series of particles defined as the boundary particles. With the same manner, the flow materials are also discretized as a range of particles with specific properties. The particle distance in this case is set to 0.75 m, which eventually makes 638,252 of boundary particles and 21,010 of fluid particles. Respect for the selection of the rheological parameters, we adopted the empirical equation via physical experiments pro-posed by Komatina and Jovanovic (1997) to derive the Bingham viscosity. In this study,

Fig. 3 2010 Yohutagawa debris-flow, Amami city, Japan (modified from KKG)

the Bingham viscosity can be analytically defined as $\mu_B = 0.621 \cdot \exp(0.173C_v)$, where C_v is the volume concentration. A previous investigation report conducted in Japan suggested the best fitted C_v is 44 %, which makes the Bingham viscosity be 1255 Pa·s. In addition, the frictional angle of the debris-flow is taken as 28° in accordance with Wu et al. (2013). Table 1 shows the main parameters run in the simulation of Yohutagawa debris-flow.

The general views of the Yohutagawa debris-flow motion in different instants are shown in Fig. 4. The results show that it takes about 30 s for the front flow to travel approximately 500 m and reach the gravity dam. The velocity of the front flow is evaluated to be maximum with an average velocity of 16 m/s. In particular, the debris does not cross over the dam in the early stage, and they are intercepted by the check dam. When exceeding the capacity of the dam, the rest materials cannot be stopped anymore and thus cross over the dam. Nevertheless, the existence of the gravity dam has dramatically slowed down the debris-flow. Therefore, in the later stage, the front flow crosses over the dam and finally remains stable at about 200 s with an average velocity of 1.5 m/s. Eventually, the debris mass out the dam is estimated to have a volume of 3510 m³, and 5353 m³ of the total mass (Table 2) is intercepted by the dam, which is in good agreement with the field investigation. Furthermore, comparing the deposition area of the simulation with that of the field investigation shown in Fig. 2c, it is obvious that the damage scope and deposition extent are modeled satisfactorily. Some differences in the deposit delineation can be partly explained by the resolution of available DEM, since the DEM data in our case were interpreted from a topographic map with the scale of 1/2000. It is believed that more precise DEM data could be helpful to obtain a better result. In addition, Fig. 5 shows the pressure field evolution of the debris-flow in different instants. It can be observed that the pressure field of the flow is smoothly produced. As previously introduced, by applying the delta-SPH, the noise of the pressure field has been efficiently corrected, especially for the flow with high viscosity.

To get further insight into the features of the debris-flow in current simulation, the average displacement and velocity time series of the particles in the flow front were analyzed. In addition, we set two sections to evaluate the discharge before and beyond the gravity dam as shown in Fig. 2c. Furthermore, we divided the deposition area into four regions shown in Fig. 2c, to analyze the flow depth distribution as compared to the field observation. Figure 6 shows the velocity time series of the front flow. Note that the data points are frequently depicted in the period of high variation. It can be obtained that in the first period of 28 s, the flow front accelerates continuously along the steep channel and peaks at about 25 m/s. Soon after, the front velocity decreases when interacting with the dam. Around 70 s, the flow starts crossing over the dam and propagating for a quite long

Table 1 Parameters run in the simulation of Yohutagawa debris-flow

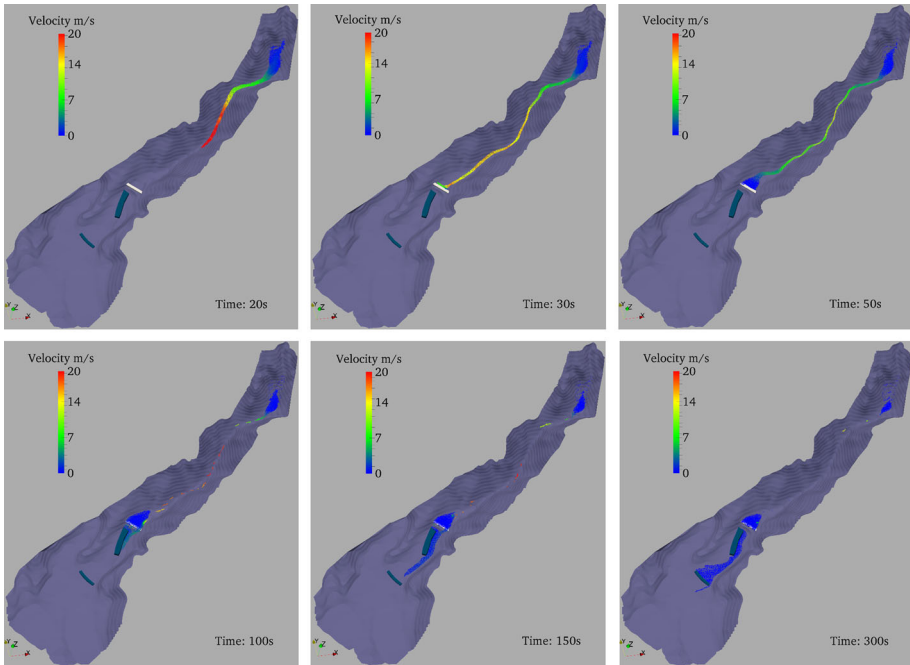| Parameters	Notation	Value
Density	ρ (kg/m³)	1650
Bingham viscosity	μ_B (Pa·s)	1255
Cohesion	c (kPa)	0
Frictional angle	φ (°)	28
Particle distance	dp (m)	0.75
No. of fluid particles	Npf	21,010
No. of boundary particles	Npb	638,252
Simulation duration	t (s)	300

Fig. 4 Snapshots of the Yohutagawa debris-flow motion in different instants

Table 2 Comparison between the calculation and field observation of the debris volume in different part

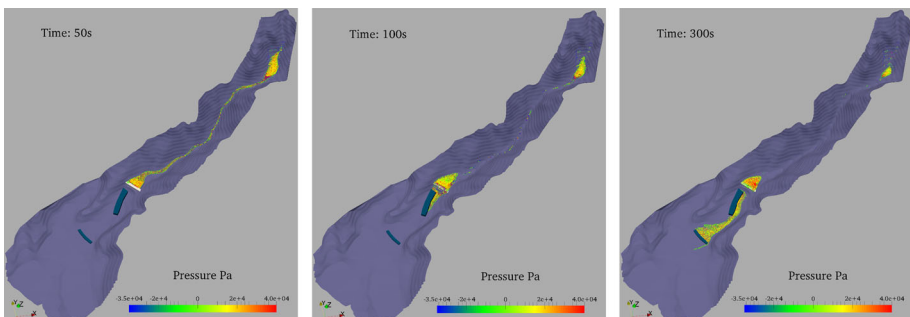| Debris volume (m^3)	Initial source	Intercept	Deposition
Calculation	8863	5353	3510
Field observation	8697	5621	3076

Fig. 5 Pressure field of the Yohutagawa debris-flow in different instants

period with the average velocity of 1.25 m/s. Since then, the flow reaches the lower building and about to be stopped. Note that the fluctuation of the velocity at some certain times indicates the complexity of the 3D terrain. Figure 7 indicates the progress of the
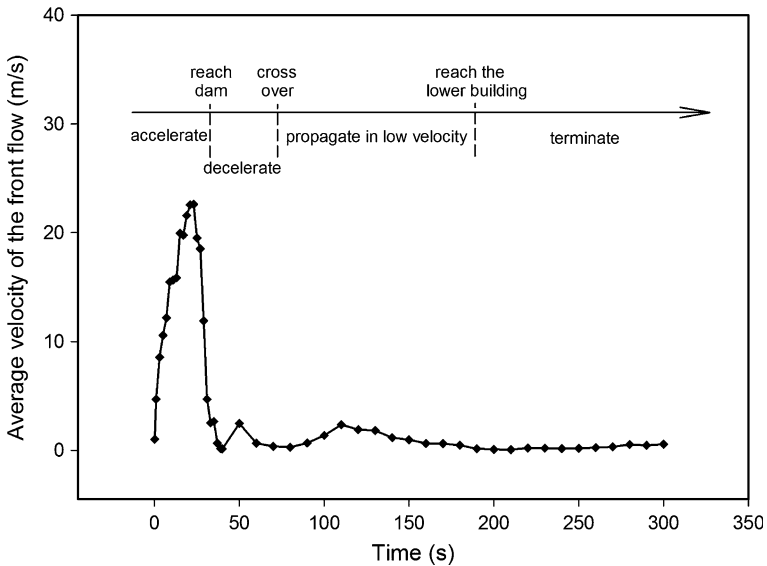
Fig. 6 Velocity time series of the front flow in the simulation

front displacement within time. The whole process can also be categorized into four stages from the initiation to termination. In summary, the debris-flow travels about 800 m from the source area to the deposition region in nearly 300 s.

Debris-flow discharge is an important parameter when designing debris-flow mitigation structures such as the deflection berms, culverts, flumes, bridges, debris-flow barriers as well as the check dams (Jakob 2005). Also, it is an essential parameter to determine the debris magnitude for hazard analysis. Figure 8 shows the estimated discharge time series of the sections set before and beyond the dam. From which, it is obtained that the maximum of the discharge in section p1 peaks at about 350 m^3/s in the initiation stage, while it gradually decreases to 80 m^3/s before reaching the check dam. On the other hand, the discharge in section p2 starts at 70 s and reaches the top of around 80 m^3/s at the time of 100 s. In terms of the depth of the deposition fan, the final result of the debris depth is visualized by MATLAB in Fig. 9. It shows that debris with maximum depth is located just before the check dam, and the debris depth in the inundation area is estimated to be 0.3 m. Table 3 shows the calculated average debris depth in different part of the deposition area comparing with those of the field observation, which proves the accuracy of the simulation in deposition analysis.

5 Discussion

As the case study outlined in Sect. 4, the SPH method incorporating the non-Newtonian behavior described by the proposed rheological model is well capable to investigate the characteristics of the debris-flow motion even across complicated 3D terrain.

The previous rheological model describing the flow-type landslide can be found in Huang et al. (2012) who accepted the Bingham model as the constitutive law. However, the limitation is that an infinite effective viscosity is arisen when the shear rate equals to
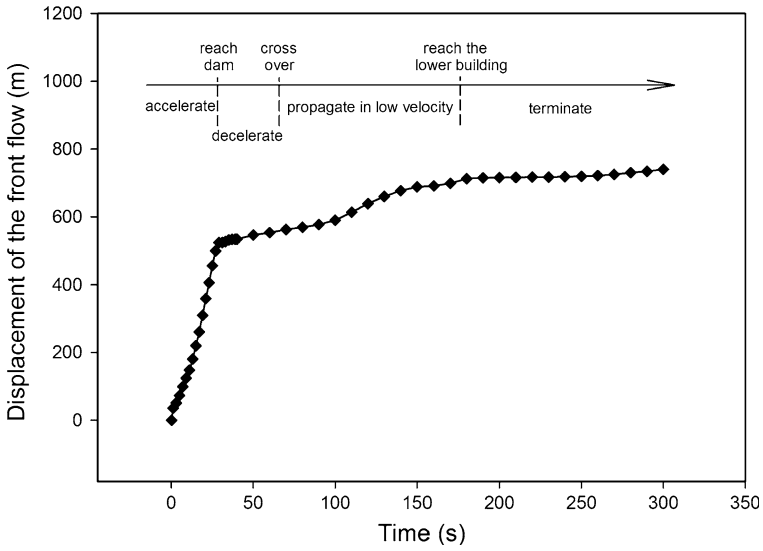
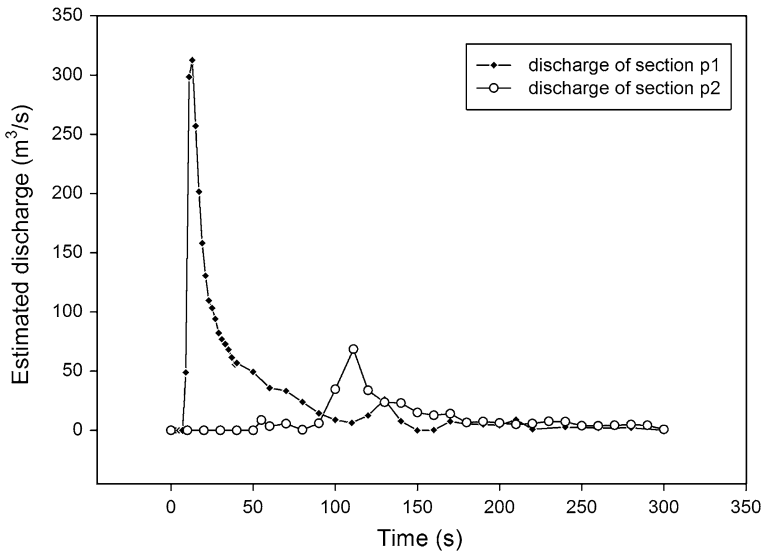**Fig. 7** Displacement time series of the front flow in the simulation

Fig. 8 Estimated discharge time series in the sections before and beyond the dam

zero. Therefore, a maximum effective viscosity threshold must be subjectively predefined and should be adjusted from case to case. In this study, for the general Cross model with parameters introduced by the Bingham model and the Mohr–Coulomb criterion, it cannot only preserve the Bingham fluid behaviors, but also ensure the numerical convergence.

As discussed by Berti and Simoni (2007), DEM resolution is very important to the performance and accuracy of the simulation, especially for in situ cases with complicated
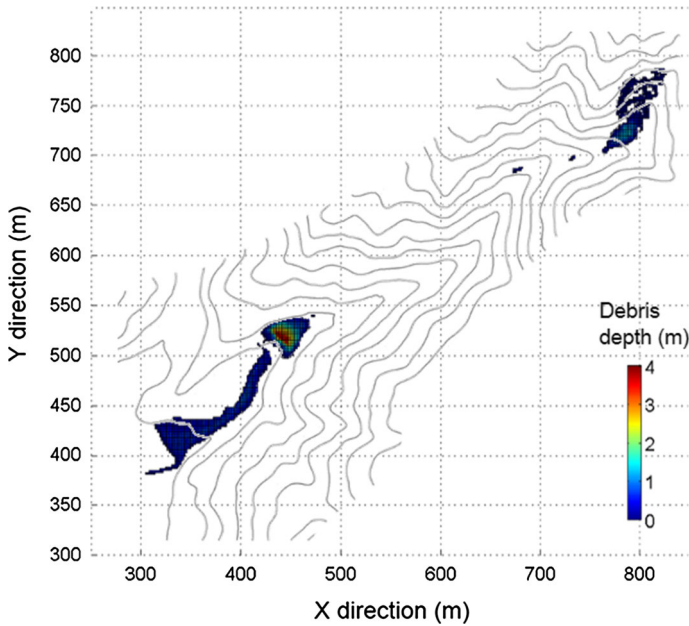
Fig. 9 Simulation result of the debris depth at $t = 300$ s

Table 3 Comparison between the calculation and field observation of the average depth in the deposition regions

Average deposition depth	Before dam		Beyond dam	
	①	②	③	④
Calculation	1.28	0.43	0.48	0.16
Field observation	1.8	0.3	0.5	0.2

3D terrain. Particularly, DEM resolution directly affects the location of the apex and inflection point of the debris channel. In fact, the motion of the debris-flow is quite sensitive to these kinds of places since huge variation in velocity and run-out is usually taken place here, as shown in Figs. 6 and 7. For instance, in our case, even using a high-resolution DEM with the scale of 1:2000, the bottom of the channel and the foothill with small variation in elevation are still poorly represented. Indeed, high-resolution DEM would be very helpful to cover the limitation if it is available. While in most case, a possible solution for this problem is to slightly adjust the unnatural parts of the flow channel according to the field topography survey.

In addition, the entrainment process of the debris-flow is not taken into account in the current study, because the multi-phases fluid has not yet been implemented. As regarded to other rheological models widely adopted in the depth-averaged equation, such as the frictional mode and Voellmy model (Hungr and McDougall 2009), they may quite suitable to deal with the rainfall-induced debris-flow. These kinds of rheological models should be implemented in future studies for different cases.

6 Conclusions

Hazard analysis and mitigation design against debris-flow require a rational modeling of flow propagation. In this study, we adopted the Navier–Stokes equations incorporating the rheological model of non-Newtonian fluid behavior to solve the dynamic motion of the flow-type landslides. The general Cross model was employed as the constitutive model, and rheological parameters were introduced from the more common Bingham model and the Mohr–Coulomb yield criterion. Subsequently, the governing equations incorporating the modified rheological model were numerically solved in the SPH framework and implemented into the DualSPHysics code which is quite robust in 3D performance.

To verify the reliability and accuracy of the modification, the 2010 Yohutagawa debris-flow event occurred in Japan was selected as the case study. A 3D model with complicated terrain corresponding to the in situ situation was created and then calculated. The calculation results were compared and in good agreements with the field observations in terms of debris volume and deposition area. It is thus concluded the proposed model is able to accurately modeling the debris-flow movement with complex topography. Besides, features such as the front velocity and section discharge of the debris-flow were also well analyzed, which will contribute to the design work of mitigation or countermeasures and provide evidences for the hazard assessment.

However, the simulation results are still affected by some uncertainties such as the DEM resolution and boundary condition. The entrainment process should also be considered in future research. Nevertheless, this SPH method-based application can be well adopted to present the debris-flow process, analyze the flow characteristics, predict the affected area and provide means for risk assessment and mitigation design.

References

Ancey C (2007) Plasticity and geophysical flows: a review. J Nonnewton Fluid Mech 142:4–35. doi:10.1016/j.jnnfm.2006.05.005

Barnes HA, Hutton JF, Walters K (1989) An introduction to rheology. Rheology series 3. Elsevier, Oxford

Berti M, Simoni A (2007) Prediction of debris flow inundation areas using empirical mobility relationships. Geomorphology 90:144–161. doi:10.1016/j.geomorph.2007.01.014

Berti M, Genevois R, Simoni A, Tecca PR (1999) Field observations of a debris flow event in the Dolomites. Geomorphology 29:265–274. doi:10.1016/S0169-555x(99)00018-5

Cascini L, Cuomo S, Pastor M, Sorbino G, Piciullo L (2012) Modeling of propagation and entrainment phenomena for landslides of the flow-type: the May 1998 case study. In: Proceedings of 11th international symposium on landslides: landslides and engineered slopes, Banf, Canada June, 2012. pp 3–8

Cascini L, Cuomo S, Pastor M (2013) Inception of debris avalanches: remarks on geomechanical modelling. Landslides 10:701–711. doi:10.1007/s10346-012-0366-0

Cascini L, Cuomo S, Pastor M, Sorbino G, Piciullo L (2014) SPH run-out modelling of channelised landslides of the flow-type. Geomorphology 214:502–513. doi:10.1016/j.geomorph.2014.02.031

Chen H, Lee C (2000) Numerical simulation of debris flows. Can Geotech J 37:146–160. doi:10.1139/Cgj-37-1-146

Cola S, Calabrò N, Pastor M (2008) Prediction of the flow-like movements of Tessina landslide by SPH model. In: Proceedings of the 10th international symposium on landslide and engineering slopes, Xi'an, China, 2008. pp 647–653

Corominas J (1996) The angle of reach as a mobility index for small and large landslides. Can Geotech J 33:260–271

Crespo A, Dominguez J, Rogers B, Gomez-Gesteira M, Longshaw S, Canelas R, Vacondio R, Barreiro A, Garcia-Feal O (2015) DualSPHysics: Open-source parallel CFD solver based on smoothed particle hydrodynamics (SPH). Comput Phys Comm 187:204–216

Crespo AC, Dominguez JM, Barreiro A, Gómez-Gesteira M, Rogers BD (2011) GPUs, a new tool of acceleration in CFD: efficiency and reliability on smoothed particle hydrodynamics methods. PLoS One 6:e20685. doi:10.1371/journal.pone.0020685

Crosta G, Dal Negro P (2003) Observations and modelling of soil slip-debris flow initiation processes in pyroclastic deposits: the Sarno 1998 event. Nat Hazards Earth Syst Sci 3:53–69

Cuomo S, Pastor M, Cascini L, Castorino GC (2014) Interplay of rheology and entrainment in debris avalanches: a numerical study. Can Geotech J 51:1318–1330. doi:10.1139/cgj-2013-0387

Dai Z, Huang Y, Cheng H, Xu Q (2014) 3D numerical modeling using smoothed particle hydrodynamics of flow-like landslide propagation triggered by the 2008 Wenchuan earthquake. Eng Geol 180:21–33. doi:10.1016/j.enggeo.2014.03.018

Dalrymple R, Rogers B (2006) Numerical modeling of water waves with the SPH method. Coast Eng 53:141–147. doi:10.1016/j.coastaleng.2005.10.004

Fannin R, Wise M (2001) An empirical-statistical model for debris flow travel distance. Can Geotech J 38:982–994

Fell R, Corominas J, Bonnard C, Cascini L, Leroi E, Savage WZ (2008) Guidelines for landslide suscepti-bility, hazard and risk zoning for land-use planning. Eng Geol 102:99–111

Frigaard I, Nouar C (2005) On the usage of viscosity regularisation methods for visco-plastic fluid flow computation. J Nonnewton Fluid Mech 127:1–26. doi:10.1016/j.jnnfm.2005.01.003

Gingold RA, Monaghan JJ (1977) Smoothed particle hydrodynamics: theory and application to non-spherical stars. Mon Not R Astron Soc 181:375–389

Gotoh H, Shao S, Memita T (2004) SPH-LES model for numerical investigation of wave interaction with partially immersed breakwater. Coast Eng J 46:39–63. doi:10.1142/S0578563404000872

Hadush S, Yashima A, Uzuoka R (2000) Importance of viscous fluid characteristics in liquefaction induced lateral spreading analysis. Comput Geotech 27:199–224. doi:10.1016/S0266-352x(00)00015-X

Hammad K, Vradis G (1994) Flow of a non-Newtonian Bingham plastic through an axisymmetric sudden contraction: effects of Reynolds and yield numbers. Numer Method Non-Newton Fluid Dyn ASME 179:63-69

Han Z, Chen G, Li Y, Zheng L, Zhang Y, Xu L (2013) A numerical simulation of volumetric enlargement for seismic debris flow using integrated DDA and KANAKO 2D. In: Frontiers of Discontinuous Numerical Methods and Practical Simulations in Engineering and Disaster Prevention. CRC Press, pp 281–287

Han Z, Chen G, Li Y, Xu L, Zheng L, Zhang Y (2014a) A new approach for analyzing the velocity distribution of debris flows at typical cross-sections. Nat Hazards 74:2053–2070. doi:10.1007/s11069-014-1276-3

Han Z, Chen G, Li Y, Zhang H, He Y (2014b) Elementary analysis on the bed-sediment entrainment by debris flow and its application using the TopFlowDF model. Geomat Nat Hazards Risk. doi:10.1080/19475705.2014.966868

Han Z, Chen G, Li Y, Tang C, Xu L, He Y, Huang X, Wang W (2015) Numerical simulation of debris-flow behavior incorporating a dynamic method for estimating the entrainment. Eng Geol 190:52–64. doi:10.1016/j.enggeo.2015.02.009

Hosseini S, Manzari M, Hannani S (2007) A fully explicit three-step SPH algorithm for simulation of non-Newtonian fluid flow. Int J Numer Meth Heat Fluid Flow 17:715–735. doi:10.1108/09615530710777976

Huang Y, Dai Z (2014) Large deformation and failure simulations for geo-disasters using smoothed particle hydrodynamics method. Eng Geol 168:86–97. doi:10.1016/j.enggeo.2013.10.022

Huang Y, Zhang W, Mao W, Jin C (2011) Flow analysis of liquefied soils based on smoothed particle hydrodynamics. Nat Hazards 59:1547–1560. doi:10.1007/s11069-011-9851-3

Huang Y, Zhang W, Xu Q, Xie P, Hao L (2012) Run-out analysis of flow-like landslides triggered by the Ms 8.0 2008 Wenchuan earthquake using smoothed particle hydrodynamics. Landslides 9:275–283. doi:10.1007/s10346-011-0285-5

Hungr O, McDougall S (2009) Two numerical models for landslide dynamic analysis. Comput Geosci 35:978–992. doi:10.1016/j.cageo.2007.12.003

Hungr O, Evans S, Bovis M, Hutchinson J (2001) A review of the classification of landslides of the flow-type. Environ Eng Geosci 7:221–238

Iverson RM (1997) The physics of debris flows. Rev Geophys 35:245–296. doi:10.1029/97rg00426

Jakob M (2005) Debris-flow hazard analysis. In: Jakob M, Hungr O (eds) Debris-flow hazards and related phenomena. Springer, Berlin, pp 411–443

Komatina D, Jovanovic M (1997) Experimental study of steady and unsteady free surface flows with water-clay mixtures. J Hydraul Res 35:579–590

Laigle D, Lachamp P, Naaim M (2007) SPH-based numerical investigation of mudflow and other complex fluid flow interactions with structures. Comput Geosci 11:297–306. doi:10.1007/s10596-007-9053-y

Lee E-S, Moulinec C, Xu R, Violeau D, Laurence D, Stansby P (2008) Comparisons of weakly compressible and truly incompressible algorithms for the SPH mesh free particle method. J Comput Phys 227:8417–8436. doi:10.1016/j.jcp.2008.06.005

Liu M, Liu G (2010) Smoothed particle hydrodynamics (SPH): an overview and recent developments. Arch Comput Methods Eng 17:25–76. doi:10.1007/s11831-010-9040-7

Liu X, Lin P, Shao S (2014) An ISPH simulation of coupled structure interaction with free surface flows. J Fluids Struct 48:46–61. doi:10.1016/j.jfluidstructs.2014.02.002

Lucy LB (1977) A numerical approach to the testing of the fission hypothesis. Astron J 82:1013–1024

Major JJ (1997) Depositional processes in large-scale debris-flow experiments. J Geol 105:345–366

McDougall S, Hungr O (2004) A model for the analysis of rapid landslide motion across three-dimensional terrain. Can Geotech J 41:1084–1097. doi:10.1139/T04-052

Medina V, Hürlimann M, Bateman A (2008) Application of FLATModel, a 2D finite volume code, to debris flows in the northeastern part of the Iberian Peninsula. Landslides 5:127–142. doi:10.1007/s10346-007-0102-3

Molteni D, Colagrossi A (2009) A simple procedure to improve the pressure evaluation in hydrodynamic context using the SPH. Comput Phys Commun 180:861–872. doi:10.1016/j.cpc.2008.12.004

Monaghan JJ (1988) An introduction to SPH. Comput Phys Commun 48:89–96. doi:10.1016/0010-4655(88)90026-4

Monaghan JJ (1992) Smoothed particle hydrodynamics. Ann Rev Astron Astrophys 30:543–574. doi:10.1146/annurev.aa.30.090192.002551

Morris JP, Fox PJ, Zhu Y (1997) Modeling low Reynolds number incompressible flows using SPH. J Comput Phys 136:214–226. doi:10.1006/jcph.1997.5776

Naili M, Matsushima T, Yamada Y (2005) A 2D Smoothed Particle Hydrodynamics method for liquefaction induced lateral spreading analysis. J Appl Mech 8:591–599

O'brien J, Julien P, Fullerton W (1993) Two-dimensional water flood and mudflow simulation. J Hydraul Eng 119:244–261

Osozawa S, Morimoto J, Flower MF (2009) "Block-in-matrix" fabrics that lack shearing but possess composite cleavage planes: a sedimentary mélange origin for the Yuwan accretionary complex in the Ryukyu island arc, Japan. Geol Soc Am Bull 121:1190–1203

Pastor M, Haddad B, Sorbino G, Cuomo S, Drempetic V (2009) A depth-integrated, coupled SPH model for flow-like landslides and related phenomena. Int J Numer Anal Meth Geomech 33:143–172. doi:10.1002/nag.705

Pastor M et al (2014) Application of a SPH depth-integrated model to landslide run-out analysis. Landslides 11:1–20. doi:10.1007/s10346-014-0484-y

Rickenmann D (1999) Empirical relationships for debris flows. Nat Hazards 19:47–77. doi:10.1023/A:1008064220727

Scheidl C, Rickenmann D (2010) Empirical prediction of debris-flow mobility and deposition on fans. Earth Surf Proc Land 35:157–173. doi:10.1002/esp.1897

Shao S (2010) Incompressible SPH flow model for wave interactions with porous media. Coast Eng 57:304–316. doi:10.1016/j.coastaleng.2009.10.012

Shao S, Lo EY (2003) Incompressible SPH method for simulating Newtonian and non-Newtonian flows with a free surface. Adv Water Resour 26:787–800. doi:10.1016/S0309-1708(03)00030-7

Sosio R, Crosta G, Frattini P (2007) Field observations, rheological testing and numerical modelling of a debris-flow event. Earth Surf Proc Land 32:290–306. doi:10.1002/esp.1391

Takahashi T, Nakagawa H, Harada T, Yamashiki Y (1992) Routing debris flows with particle segregation. J Hydraul Eng 118:1490–1507. doi:10.1061/(Asce)0733-9429(1992)118:11(1490)

Tang C, Rengers N, van Asch TW, Yang Y, Wang G (2011) Triggering conditions and depositional characteristics of a disastrous debris flow event in Zhouqu city, Gansu Province, northwestern China. Nat Hazards Earth Syst Sci 11:2903–2912. doi:10.5194/nhess-11-2903-2011

Wang G, Sassa K, Fukuoka H (2003) Downslope volume enlargement of a debris slide–debris flow in the 1999 Hiroshima, Japan, rainstorm. Eng Geol 69:309–330. doi:10.1016/S0013-7952(02)00289-2

WU J, Chen G, Zheng L, Zhang Y (2013) GIS-based numerical modelling of debris flow motion across three-dimensional terrain. J Mt Sci 10:522–531. doi:10.1007/s11629-013-2486-y